



# Prognostication of scour around twin and three piers using efficient outlier robust extreme learning machine

Mohammad Rashki Ghaleh Nou<sup>1</sup> · Ali Foroudi<sup>2</sup> · Sarmad Dashti Latif<sup>3</sup> · Abbas Parsaie<sup>4</sup>

Received: 20 February 2022 / Accepted: 3 May 2022 / Published online: 31 May 2022  
© The Author(s), under exclusive licence to Springer-Verlag GmbH Germany, part of Springer Nature 2022

## Abstract

One of the most essential difficulties in the design and management of bridge piers is the estimation and modeling of scouring around the piers. The scour depth downstream of twin and three piers were simulated using a new outlier robust extreme learning machine (ORELM) model in this study. Furthermore,  $k$ -fold cross-validation with  $k=4$  was employed to validate the outcomes of numerical models. Four ORELM models with effective scouring parameters were first created to simulate scour depth. After then, the number of hidden layer neurons increased from two to thirty. The number of ideal hidden neurons was determined by examining the modeling results. The sigmoid activation function was also introduced as the best function. Furthermore, a sensitivity analysis was used to identify the superior model. The best model predicted scour depth as a function of the Froude number ( $Fr$ ), the pier diameter to flow depth ratio ( $D/h$ ), and the distance between the piers to flow depth ratio ( $d/h$ ). The values of the objective function were accurately approximated by this model. As a result, using the ORELM model, the  $R^2$ , scatter index, and Nash–Sutcliffe efficiency coefficient were calculated to be 0.953, 0.146, and 0.949, respectively. The most efficient parameters for simulating the scour depth were  $Fr$  and  $D/h$ , according to the modeling results. It is worth noting that nearly half of the superior model's simulated outputs had an inaccuracy of less than 10%. The superior model's performance has been underestimated, according to uncertainty analysis. After that, a simple and practical equation for calculating the scour depth was established for the superior model. Additionally, the influence of each input parameter on the objective function was assessed using a partial derivative sensitivity analysis.

**Keywords** Outlier robust extreme learning machine (ORELM) · Scour · Twin and three piers · k-fold Cross-validation · Uncertainty analysis · Partial derivative sensitivity analysis

Responsible Editor: Philippe Garrigues

✉ Ali Foroudi  
aliforoudi@qiet.ac.ir

Mohammad Rashki Ghaleh Nou  
mohammadrashki@yahoo.com

Sarmad Dashti Latif  
Sarmad.latif@komar.edu.iq

Abbas Parsaie  
parsaie@scu.ac.ir

<sup>1</sup> Department of Civil Engineering, University of Sistan and Baluchestan, Zahedan, Iran

<sup>2</sup> Department of Civil Engineering, Faculty of Engineering, Quchan University of Technology, Quchan, Iran

<sup>3</sup> Civil Engineering Department, College of Engineering, Komar University of Science and Technology, Sulaimany 46001, Kurdistan Region, Iraq

<sup>4</sup> Faculty of Water and Environmental Engineering, Shahid Chamran University of Ahvaz, Ahvaz, Iran

## Introduction

The water flow around hydraulic constructions like piers, abutments, and weirs causes the scouring phenomena. The development of a vacuum at the interface of the two media (sediment and fluid) due to the velocity gradient is the cause of this phenomenon. Scouring occurs in the region of bridges, abutments, downstream of the Ogee spillways, and submerged spillways, among other structures. These structures have a high chance of being destroyed if the scour hole size is increased. The restoration and rehabilitation of numerous buildings, particularly bridge piers damaged by scouring, cost a lot of money every year. As a result, assessing and predicting the proportions and pattern of scouring around bridge piers are critical, and numerous studies have been conducted in this area (Harasti et al. 2021; Link et al. 2019).

It should be mentioned that many studies on the scour pattern around complex piers and pier groups have also been conducted. Coleman (2005) undertook an experiment to measure the scour around the intricate piers. They developed a method for calculating the minimum and maximum local scouring in the area of complex piers. Melville et al. (2007) have provided an analytical method for calculating the diameters of scour holes around complex piers. They validated their model's conclusions with experimental data, demonstrating that this strategy is accurate enough. In the following paper, Ataie-Ashtiani et al. (2010) tested the scour depth under the vicinity of complex piers in clear-water conditions. They discovered that when the pile cap was undercut, the maximum scour depth occurred. In an experimental investigation, Amini et al. (2012) investigated the scour pattern around pier groups in clear water in shallow waters. Moreno et al. (2016) carried out an experiment to quantify the scour around the complex piers in clear-water flow conditions. They discovered that when a portion of the pile cap is buried in the sediments, the maximum scour depth occurs. F. Liang et al. (2017) also investigated the scour hole depth surrounding the single, twin, and pier groups experimentally. They claimed that the scour pattern around single piers differs significantly from that surrounding pier groupings. Amini Baghbadorani et al. (2017) used empirical relationships to examine experimental values gathered in the area of pier groups in earlier investigations. They devised an equation to compute the scour depth around the pier groups, claiming that the equation's accuracy was around 10% higher than that of prior research. The scouring pattern around the pier groups and complex piers was studied by Amini Baghbadorani et al. (2018). They demonstrated that the scour pattern changes around pier groups and complex piers, and they established distinct equations for calculating scouring for these two types of structures. The effects of inclination angle on the scour pattern in the vicinity of two types of pier groups were investigated by Bozkuş et al. (2018). They evaluated the findings and gave some empirical equations for determining scour around pier groups.

Various investigations on the scouring pattern around twin and three piers have also been conducted. Ataie-Ashtiani and Aslani-Kordkandi (2012) measured the scouring pattern around twin bridge piers. They discovered that between the two bridge piers, the bed shear stress was higher than in other regions. In addition, in an experimental investigation, Das et al. (2016) looked at the scour values around the twin piers with circular, square, and triangular cross sections. They claimed that the scour hole length near the triangular twin piers was shorter than that near the circular and square piers. Wang, et al. (2016a, b) also conducted an experiment to determine the scour depth at the circular twin pier. They discovered that the scour depth around the downstream pier was lower than

the scour depth around the upstream pier by examining the testing findings. In an experimental investigation, Wang, et al. (2016a, b) looked at the scouring values around three piers of the same distance. They conducted the tests in clear water and found that the scour depth around the upstream pier was the same as that around the single pier.

Nowadays, artificial intelligence techniques have been widely used for many engineering applications (Bazrafshan et al. 2022; Ehteram et al. 2020; Latif 2021a, 2021b; Latif et al. 2020; Latif et al., 2021a, 2021b; Latif, Birima, et al. 2021a, b; Latif and Ahmed 2021; Najah et al. 2021; Parsaie and Haghiabi 2017; Parsaie et al. 2021). Also, artificial intelligence techniques have been used for scour around bridge piers prediction, for example, Etemad-Shahidi et al. (2015) used the M5 model tree to simulate the scour depth around the bridge piers. They discovered that the M5 model tree outperformed the empirical relationships after assessing the modeling findings. Muzzamil et al. (2015) used the Gene Expression Programming (GEP) model to estimate the scour hole size in cohesive sediments around bridge piers. They compared the results of their numerical model to the experimental findings and found that the GEP model outperformed the nonlinear regression model in terms of accuracy. Azimi et al. (2017) created a hybrid model for simulating scour depth in the vicinity of pier groups utilizing Adaptive Neuro-Fuzzy Inference System (ANFIS), Singular Decomposition Value (SVD), and Differential Evolution (DE) methods. They demonstrated that the hybrid model was accurate enough. Using the Extreme Learning Machine (ELM) model, Ebtahaj et al. (2018) projected scour depth at the pier groups. They also compared their findings to those of artificial neural networks (ANN) and support vector machines (SVM), finding that the ELM model was more accurate.

Artificial neural networks (ANNs) are believed to be very popular and practical approaches based on the results of earlier studies and their acceptable performance in tackling nonlinear problems that are difficult to solve using traditional analytical and numerical methods. Although this strategy has demonstrated accurate results in multiple trials, it also has several drawbacks, the most significant of which is the slow training speed. The slow learning speed of ANN models is caused by the slowness of gradient algorithms and the repeated setting of ANN parameters throughout the training phase. By transforming a nonlinear problem into a linear problem, the extreme learning machine (ELM) method has solved the problem of high-speed modeling in a single-layer feed-forward neural network (SLFFNN) (Huang et al. 2004). Furthermore, this strategy is highly generalizable (N. Y. Liang et al. 2006). Although ELM models have numerous advantages, they tend to outlier data throughout the training phase, reducing the model's accuracy and validity (Horata et al. 2013).

Zhang and Luo (2015) proposed outlier robust ELM (ORELM) approaches to address this issue.

Artificial intelligence techniques, such as ELM and its expanded forms (i.e., ORELM), are, on the other hand, frequently employed by researchers and engineers. Artificial intelligence technologies, on the other hand, have not been used to simulate and estimate scouring in the region of twin and three piers. As a result, a new ORELM approach is used to model the scour depth around the twin and three piers in this study. The optimal number of hidden neurons is chosen utilizing the trial-and-error method to attain this goal. For modeling the scour depth, the optimum activation function is also introduced. It should be mentioned that the  $k$ -fold cross-validation approach with  $k = 4$  is utilized to check the numerical model's results. In addition, the input parameters are used to create four different ORELM models. The superior model and effective parameters are chosen using sensitivity analysis. Error analysis and uncertainty analysis are also implemented in ORELM models. The superior model is then given a realistic and straightforward relationship. A partial derivative sensitivity analysis is performed for this equation.

## Material and methods

### Experimental model

The experimental data of Wang, et al. (2016a, b) and Wang, et al. (2016a, b) were used in this investigation to develop the soft computing model. A rectangular flume with length, width, and height of 12, 0.42, and 0.7 m is included in the experimental model. Two piers with a diameter of 6 cm were built in the twin pier type. It should be mentioned that the sediment layer had an initial depth of 15 cm and a length of 6 m, and twin piers were positioned in the sediment layer at a distance of  $d$ . The distance between the piers was assumed to be between 0 and 15 times the pier diameter in the three piers model. Figure 1 depicts a schematic representation of Wang, et al. (2016a, b) and Wang, et al. (2016a, b) experimental models.

### Scour around piers

The scour depth in the vicinity of the pier groups ( $ds$ ) is a function of the mean diameter of the sediment particles ( $d_{50}$ ), the number of piers parallel to the flow direction ( $m$ ), the diameter of the bridge piers ( $D$ ), the center-to-center distance between bridge piers in the direction parallel to the flow ( $d$ ), the center-to-center distance between bridge piers in the direction perpendicular to the flow ( $Sn$ ), flow depth ( $h$ ), average flow:

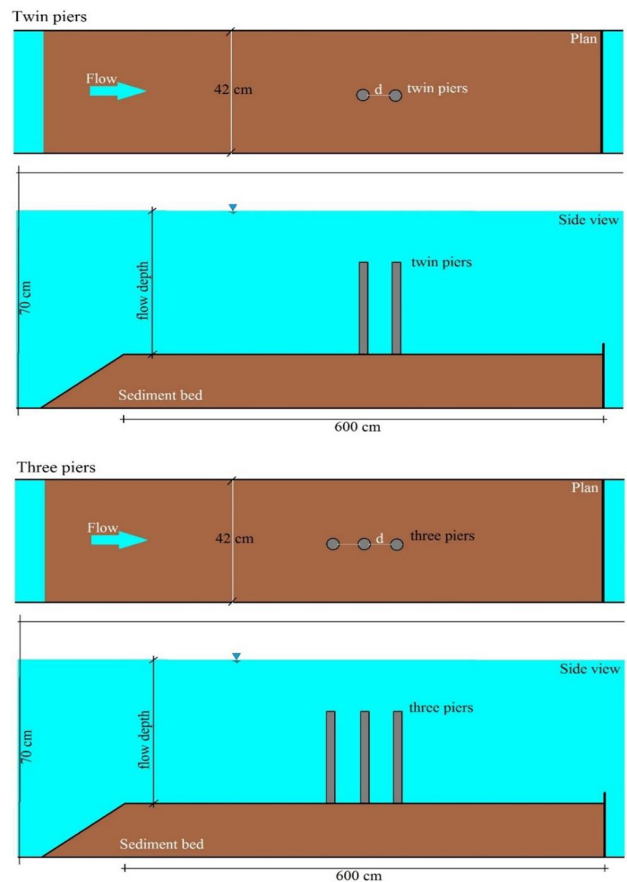


Fig. 1 Schematic representation of Wang et al. (2016a) and Wang et al. (2016b) experimental models (2016b)

$$ds = f(d_{50}, m, n, D, d, S_n, h, U, U_c) \quad (1)$$

where  $U$  is the mean vertical velocity of the approaching flow, and  $U_c$  is the incipient velocity of sediment motion. Wang, et al. (2016a, b) and Wang, et al. (2016a, b) used a distance of  $d$  to measure the scour around the piers. The values of  $d_{50}$ ,  $m$ ,  $n$ ,  $d$ ,  $S_n$ , and  $U_c$  in their investigation were nearly constant. When the dimensionless parameters are considered, Eq. 1 is rewritten as follows:

$$ds/h = f(D/h, d/h, Fr) \quad (2)$$

$Fr$  is the Froude number in this case. As a result, the parameters of Eq. 2 are used as input parameters in numerical models in this work. Figure 2 depicts the input parameter combinations for several models. In addition, Table 1 shows the range of experimental values used in this investigation.

### ELM

Huang et al. (2004) developed ELM, which is an SLFFNN training method. In actuality, SLFFNN is a linear system

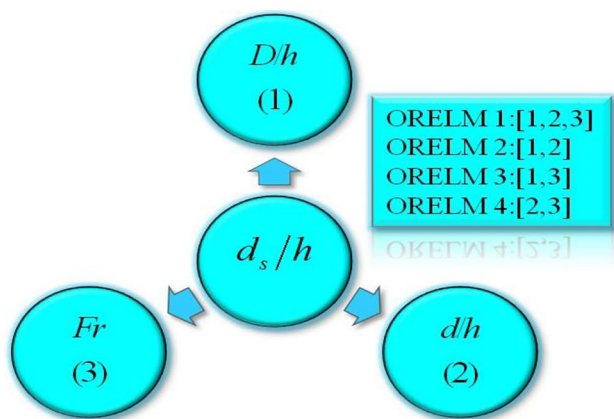


**Fig. 2** ORELM model development using a combination of input parameters

**Table 1** Experimental values range utilized in this study

Parameter	Maximum	Minimum	Average	Standard deviation	Variance
<i>ds/h</i>	0.625	0.008	0.227	0.152	0.023
<i>D/h</i>	0.500	0.250	0.359	0.107	0.011
<i>d/h</i>	7.50	0.250	2.588	1.954	3.817
<i>Fr</i>	0.258	0.116	0.186	0.040	0.002

in which the input weights for hidden neurons and hidden layer biases are chosen at random, but the weights between hidden nodes are calculated analytically. This technique outperforms traditional learning algorithms in terms of performance and learning speed (Huang et al. 2004). Because, unlike traditional methods that necessitate the adjustment of numerous parameters, this method does not necessitate extensive human interaction to attain optimal values (Ebtehaj et al. 2016). The following is a representation of a standard single-layer neural network with  $N$  random data  $(x_i, t_i)$ ,  $N$  hidden neurons, and the active function  $g(x)$ :

$$x_i = [x_{i1}, x_{i2}, \dots, x_{in}]^T \in R^n \tag{3}$$

$$x_i = [x_{i1}, x_{i2}, \dots, x_{in}]^T \in R^n \tag{4}$$

$$t_i = [t_{i1}, t_{i2}, \dots, t_{in}]^T \in R^m \tag{5}$$

$$\sum_{i=1}^N \beta_i g(w_i x_j + b_i) = o_j, j = 1, 2, \dots, N \tag{6}$$

in which,  $w_i = [w_{i1}, w_{i2}, \dots, w_{in}]^T$  is the weight vector connecting the hidden neurons to the input neurons;  $\beta_i = [\beta_{i1}, \beta_{i2}, \dots, \beta_{in}]^T$  represents the weight vector connecting the

hidden neurons to the output neurons;  $b_i$  is the biases of the hidden neurons;  $w_i x_j$  indicates the internal multiplication of  $w_i$  and  $x_j$ . The standard SLFFNN network with the  $N$  hidden neurons and the activation function  $g(x)$  can estimate  $N$  data with a zero error ( $\sum_{j=1}^N \|o_j - t_j\| = 0$ ), in which.

$$\sum_{i=1}^N \beta_i g(w_i x_j + b_i) = t_j, j = 1, 2, \dots, N \tag{7}$$

The above equations can be rewritten as follows:

$$H\beta = T \tag{8}$$

$$H(w_1, \dots, w_N, b_1, \dots, b_N, x_1, \dots, x_N) = \begin{bmatrix} g(w_1 \cdot x_N + b_1) & \dots & g(w_N \cdot x_1 + b_N) \\ \vdots & \vdots & \vdots \\ g(w_1 \cdot x_N + b_1) & \dots & g(w_N \cdot x_N + b_N) \end{bmatrix}_{N \times N} \tag{9}$$

$$\beta = \begin{bmatrix} \beta_1^T \\ \vdots \\ \beta_N^T \end{bmatrix}_{N \times m} \tag{10}$$

$$T = \begin{bmatrix} t_1^T \\ \vdots \\ t_N^T \end{bmatrix}_{N \times m} \tag{11}$$

The matrix  $H$  is called the output matrix of the hidden layers of the neural network. The  $i^{\text{th}}$  column of the matrix  $H$  represents  $i^{\text{th}}$  vector of the output of the hidden neurons (considering  $x_1, x_2, \dots, x_N$  as input).

The determination of the input weights ( $w_i$ ) and the hidden layer biases ( $b_i$ ) are equivalent to finding a solution for  $\beta$  least square of the linear system  $H\beta = T$ .

$$\|H(w_1, \dots, w_N, b_1, \dots, b_N)\beta - T\| = \min_{\beta} \|H(w_1, \dots, w_N, b_1, \dots, b_N)\beta - T\| \tag{12}$$

The least average solution for the least square of the linear system is

$$\beta = H^+ T. \tag{13}$$

### ORELM

In addition to the general form of ELM, the following cases should be considered in the ORELM technique (Zhang and Luo 2015):

$C$ , a new adjustment parameter, is introduced. The ratio of the training error to the output weight norm is this parameter. This parameter can be used to concurrently minimize the training error and the output weight norm; in other words, it can be used to increase the model’s generalizability performance

when compared to the ELM model, which is represented by the equation:

$$\min_{\beta} C \|T - H\beta\|_2^2 + \|\beta\|_2^2. \tag{14}$$

The scattering can be better reflected using  $\ell_0$ -norm instead of  $\ell_2$ -norm. Hence, the output weight  $\beta$  is considered with a smaller  $\ell_2$ -norm, so that the training error  $e$  is reduced; that is:

$$\min_{\beta} C \|e\|_0 + \|\beta\|_2^2 \text{ subject to } T - H\beta = e. \tag{15}$$

A non-convergent programming problem is the one shown above. Refreshing the issue with a tractable form relaxation convex without losing the dispersion index is a simple technique to solve it. The dispersion feature is ensured by replacing the  $\ell_1$ -norm with the  $\ell_0$ -norm, resulting in maximum convergence. As a result, the equation looks like this:

$$\min_{\beta} \|e\|_1 + \frac{1}{C} \|\beta\|_2^2 \text{ subject to } T - H\beta = e \tag{16}$$

where, the augmented Lagrangian function is defined as follows:

$$L_{\mu}(e, \beta, \lambda) = \|e\|_1 + \frac{1}{C} \|\beta\|_2^2 + \lambda^T(T - H\beta - e) + \frac{\mu}{2} \|T - H\beta - e\|_2^2 \tag{17}$$

where  $\mu$  is the error parameter and  $\lambda$  is the augmented Lagrangian vector. According to Yang and Zhang (2011), the value of  $\mu$  should be assumed to be  $\mu = 2N/\|T\|$ . The ideal response ( $e, \beta$ ) and the coefficient  $\lambda$  are computed in the augmented Lagrange multiplier (ALM) by repeating to minimize the completed Lagrangian function. In summary, the repeat design of ALM, according to  $(\lambda_k, \mu)$ , is as follows:

$$\begin{cases} (e_{k+1}, \beta_{k+1}) = \arg \min_{e, \beta} L_{\mu}(e, \beta, \lambda_k) \\ \lambda_{k+1} = \lambda_k + \mu(T - H\beta_{k+1} - e_{k+1}). \end{cases} \tag{18}$$

These equations can be rewritten as follows:

$$\begin{cases} \beta_{k+1} = \arg \min_{\beta} L_{\mu}(e_k, \beta, \lambda_k) \\ \beta_{k+1} = \arg \min_{\beta} L_{\mu}(e_k, \beta, \lambda_k) \\ \lambda_{k+1} = \lambda_k + \mu(T - H\beta_{k+1} - e_{k+1}) \end{cases} \tag{19}$$

**Goodness of fit**

The statistical indices of determination coefficients ( $R^2$ ), variance accounted for (VAF), root mean square error (RMSE), scatter index (SI), mean absolute error

(MAE), mean absolute relative error (MARE), and Nash–Sutcliffe efficiency coefficient (NSC) are used in this study to evaluate the accuracy of numerical models:

$$R^2 = \frac{(n \sum_{i=1}^n P_i O_i - \sum_{i=1}^n P_i \sum_{i=1}^n O_i)^2}{(n \sum_{i=1}^n (P_i)^2 - \sum_{i=1}^n (P_i))^2 (n \sum_{i=1}^n (O_i)^2 - \sum_{i=1}^n (O_i))^2} \tag{20}$$

$$VAF = \left(1 - \frac{\text{var}(P_i - O_i)}{\text{var}(P_i)}\right) \times 100 \tag{21}$$

$$RMSE = \sqrt{\frac{1}{n} \sum_{i=1}^n (P_i - O_i)^2} \tag{22}$$

$$SI = \frac{RMSE}{\bar{O}} \tag{23}$$

$$MAE = \frac{\sum_{i=1}^n |P_i - O_i|}{n} \tag{24}$$

$$MARE = \frac{1}{n} \sum_{i=1}^n \frac{|P_i - O_i|}{O_i} \tag{25}$$

$$NSC = 1 - \frac{\sum_{i=1}^n (O_i - P_i)^2}{\sum_{i=1}^n (O_i - \bar{O})^2} \tag{26}$$

where  $O_i$  denotes the observed values,  $P_i$  denotes the numerical models' simulated values,  $\bar{O}$  is the average of observational values, and  $n$  denotes the number of observational values.

Because the statistical indices offered do not allow for simultaneous comparison of the models' mean and variance, the Akaike information criterion (AIC) is used to compare the predicted discharge coefficient to the experimental value (Ebtehaj et al. 2016):

$$AIC = n \cdot \log \left[ \frac{1}{n} \sum_{i=1}^n (R_{(Observed)_i} - R_{(Predicted)_i})^2 \right] + 2k \tag{27}$$

The number of estimated parameters employed in the numerical model is given by  $k$ . The ACI parameter is used as a benchmark for determining how well a statistical model adapts. It is also used to choose a model, and it describes the numerical model's complexity and accuracy at the same time.

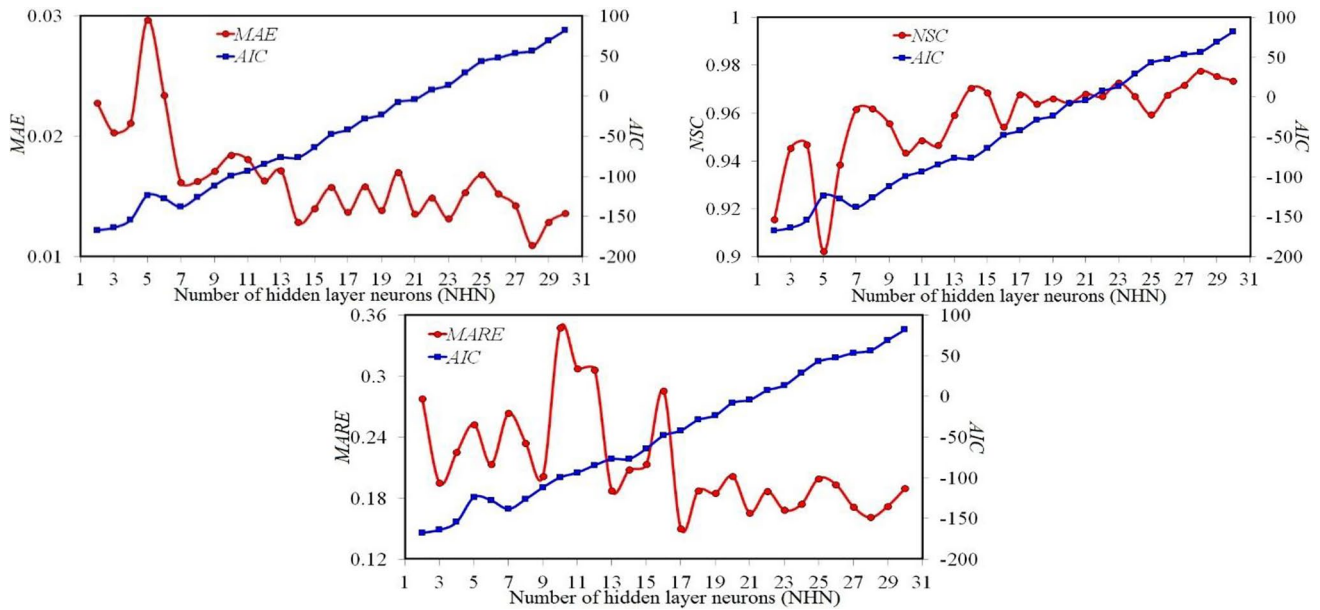


Fig. 3 The number of hidden neuron layers varies according to different statistical parameters

## Results and discussion

### Number of hidden layer neurons

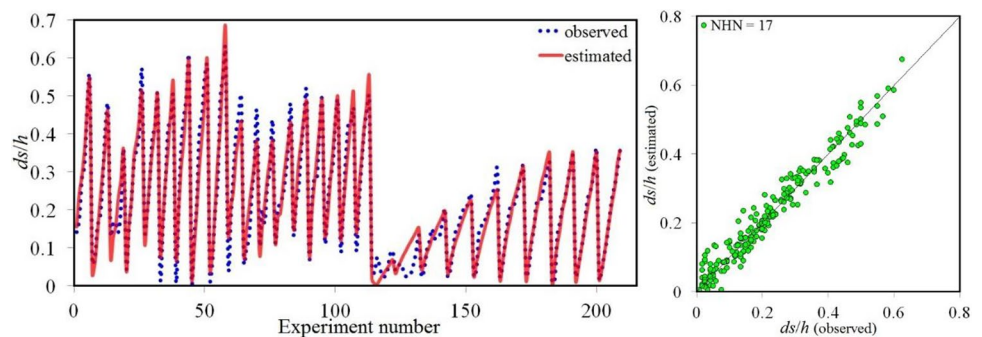
First, the number of hidden layer neurons is examined. Figure 3 depicts the relationship between the number of hidden layer neurons and numerous statistical indices. Two criteria must be considered when determining the ideal number of hidden layer neurons. (1.) The AIC value is the smallest, and (2.) the MARE value is less than 0.15. The number of hidden layer neurons was first estimated to be two, then increased to thirty. The numerical model considers the number of ideal hidden layer neurons to be 17 based on these two criteria. For example, when NHN equals 15, the numerical model’s MARE and AIC values were calculated to be 0.150 and  $-41.807$ , respectively. Furthermore, the VAF, RMSE, and NSC values for these hidden neuron layers were estimated to be 99.758, 0.018, and 0.968, respectively.

The scatter plot and comparison of observed and simulated values for  $NHN = 17$  are shown in Fig. 4.  $R^2$ , MAE, and SI are computed as 0.968, 0.014, and 0.096, respectively, for a model with  $NHN = 17$ . As a result, the best number of this parameter was determined to be 17 based on the number of hidden layer neurons.

### Activation function selection

The correctness of the numerical model’s numerous activation functions is assessed in this section. Sig, sin, radbas, tribas, and hardlim are the five activation functions in the ELM model. Figure 5 depicts the findings of statistical indicators. The VAF, SI, and RMSE values for the sig activation function are 96.758, 0.096, and 0.018, respectively. Meanwhile, for the sin activation function, the MAE and SI indices are 0.016 and 0.011, respectively. The RMSE, NSC, and VAF indices for the radbas activation function are 0.039, 0.909, and 85.803 correspondingly. The values of SI, MAE, and RMSE for the tribas

Fig. 4 Scatter plot with simulated and observed scouring values for  $NHN = 17$



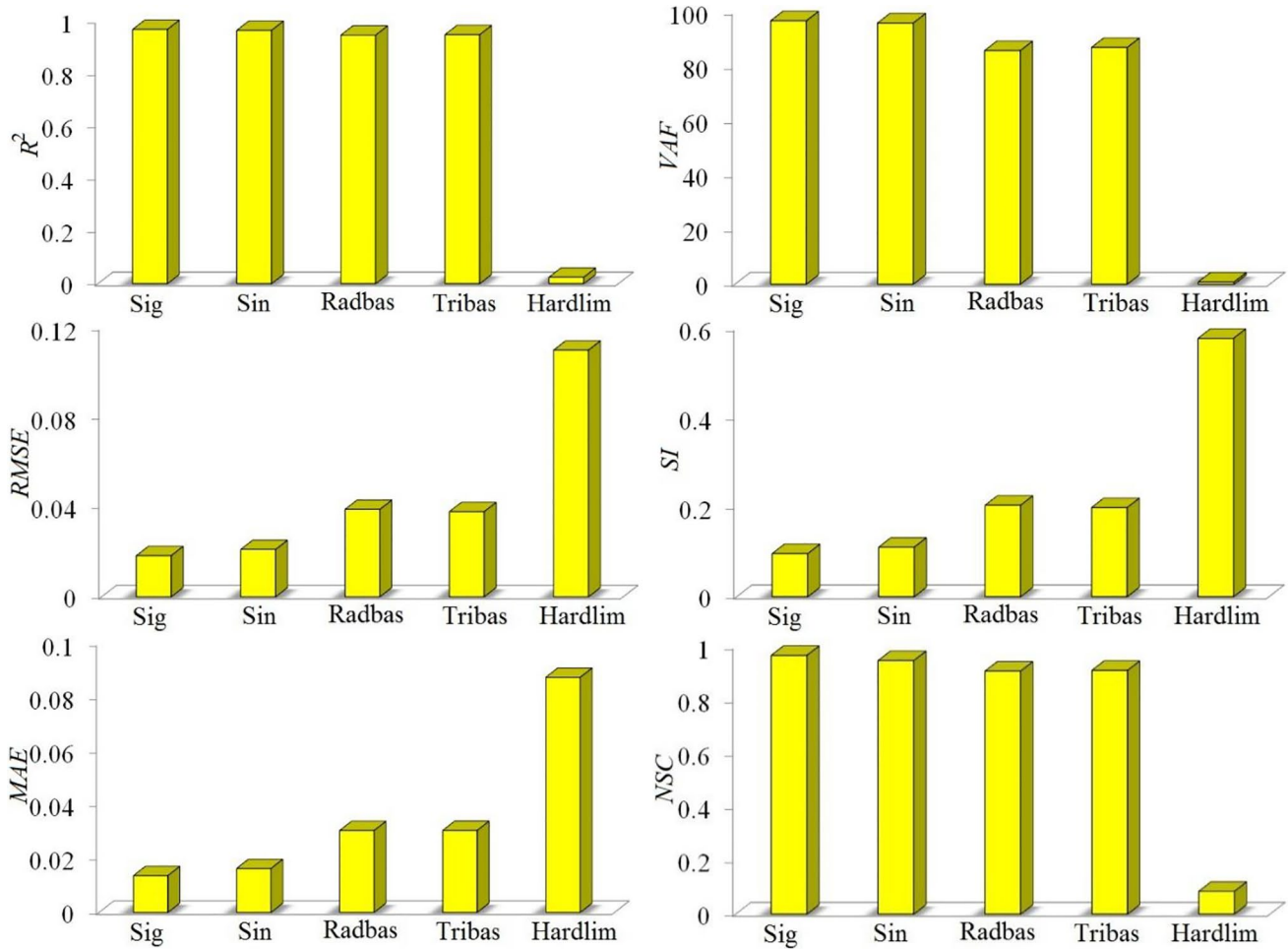


Fig. 5 Results of statistical indices for various activation functions

Table 2 Error indices of tested activation functions of ELM model

Activation function	$R^2$	VAF	RMSE	SI	MAE	NSC
Sig	0.98	97	0.02	0.10	0.144	0.98
sin	0.96	95	0.02	0.11	0.176	0.96
radbas	0.91	86	0.04	0.20	0.32	0.91
tribas	0.92	88	0.04	0.20	0.32	0.92
hardlim	0.10	2	0.11	0.58	0.896	0.09

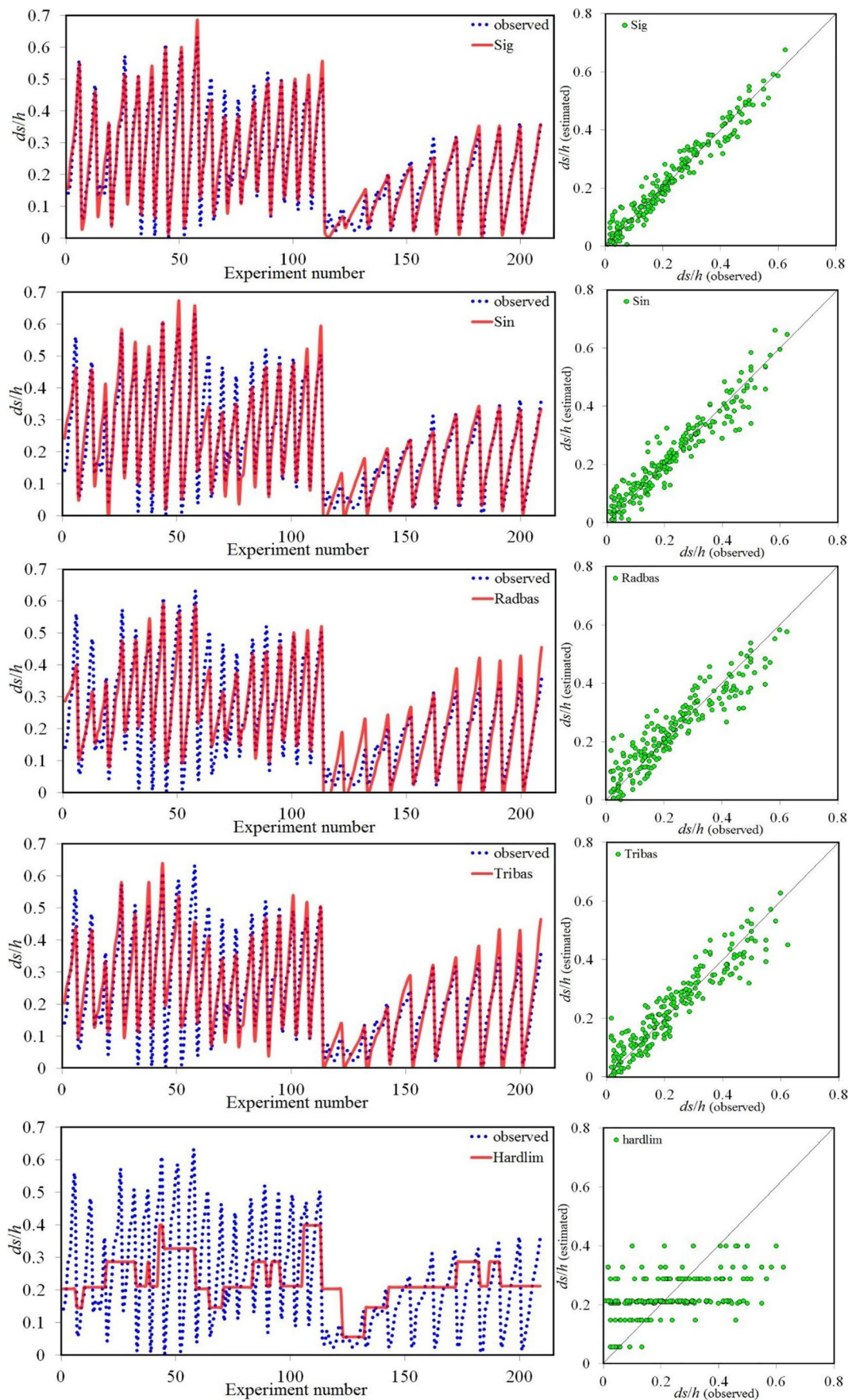
activation function, on the other hand, are 0.199, 0.030, and 0.038, respectively. The VAF and SI values for the hardlim function are estimated to be 0.831 and 0.578, respectively, based on the findings of the activation functions. The error indices of activation functions tested during the development of ELM model are given in Table 2.

Figure 6 also shows scatter plots and outcomes of scouring simulations using various activation functions. The  $R^2$  values for the activation functions sig, sin, and radbas, for example, are 0.968, 0.964, and 0.946, respectively. Furthermore, the amount of  $R^2$  for tribas and hardlim functions was

estimated to be 0.948 and 0.024, respectively. As a result, the sig function is identified as the superior activation function based on the findings of the activation functions.

**k-fold cross-validation**

The data is separated into  $k$  subgroups in this type of validation. One subset is utilized for validation, and the other  $k - 1$  subsets are used for training. This process is repeated, with all data being utilized twice for training and validation. Finally, as a final estimate, the average result of  $k$  times





**Fig. 6** Scatter plot and comparison of observed and simulated scouring values

validation is chosen. For  $k=4$ , Fig. 7 depicts the  $k$ -fold cross-validation procedure. Figure 8 depicts the scatter plots for the four validation stages of the  $k$ -fold cross-validation approach. The  $R^2$  values for  $k=1$  and  $k=2$  in the test mode are 0.949 and 0.952, respectively. The  $R^2$  values for  $k=3$  and  $k=4$  are calculated to be 0.953 and 0.950, respectively.

### Performance of ORELM models

The findings of the ORELM 1 to ORELM 4 models are presented in this part to simulate the scour depth around twin and three piers. Figure 9 depicts the findings of various statistical indices for these models. For all input parameters ( $D/h$ ,  $d/h$ , and  $Fr$ ), the ORELM model calculates the scour depths. The VAF and RMSE statistical indices have been calculated to be 95.249 and 0.033, respectively, for this model, while this model's scatter index is 0.146.

Three ORELM 2 to ORELM 4 models, on the other hand, estimate the values of the objective function using the three input parameters. The ORELM 2 model, for example, is a function of  $D/h$  and  $d/h$ . The statistical indices of MAE, SI, and RMSE for this model are 0.099, 0.549, and 0.125, respectively.

ORELM3's SI, VAF, and NSC values are also predicted to be 0.245, 84.316, and 0.814, respectively. The effect of the  $d/h$  has been removed from this model. In other words, the model uses  $D/h$  and Froude numbers to estimate the values of the goal function.

Furthermore, because the ORELM4 model is a function of  $d/h$  and  $Fr$ , the effect of the  $D/h$  parameter is neglected. MAE, VAF, and RMSE for ORELM4 are calculated to be 0.056, 75.284, and 0.076, respectively. The NSC for this model is equivalent to 0.671.

Figures 10 and 11 provide a comparison of simulated and observed scouring values, as well as error distribution diagrams for ORELM models. The  $R^2$  coefficient for the

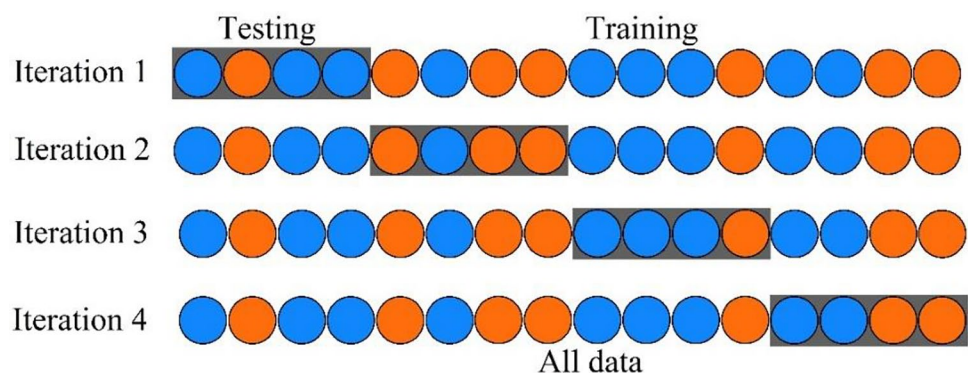
ORELM model is 0.953. Furthermore, the ORELM1 model simulates nearly half of the scouring values with an inaccuracy of less than 10%. It is worth noting that around a third of the ORELM1 model's outputs have an inaccuracy of more than 15%. The  $R^2$  score for the ORELM2 model is 0.326. Approximately 81% of the outcomes for this model have a margin of error greater than 15%. It should be noted that around 8% of the scouring values simulated by ORELM2 have an inaccuracy of 10 to 15%. Furthermore, the  $R^2$  value for the ORELM3 model is predicted to be 0.843, and around 32% of the findings have an error of less than 10%. In comparison, around 68% of the values estimated using the ORELM4 model have an error greater than 15%, and 9% of the findings have an error between 10 and 15%. The  $R^2$  value for ORELM is approximately 0.753.

As a result of the modeling results, the ORELM1 model is determined to be the superior model. In terms of  $D/h$ ,  $d/h$ , and  $Fr$ , this model calculates the scour depths in the vicinity of twin and three piers. The parameters of the Froude number ( $Fr$ ) and the ratio of the pier diameter to the flow depth ( $D/h$ ) were also found as the most effective input parameters after an analysis of the simulation results.

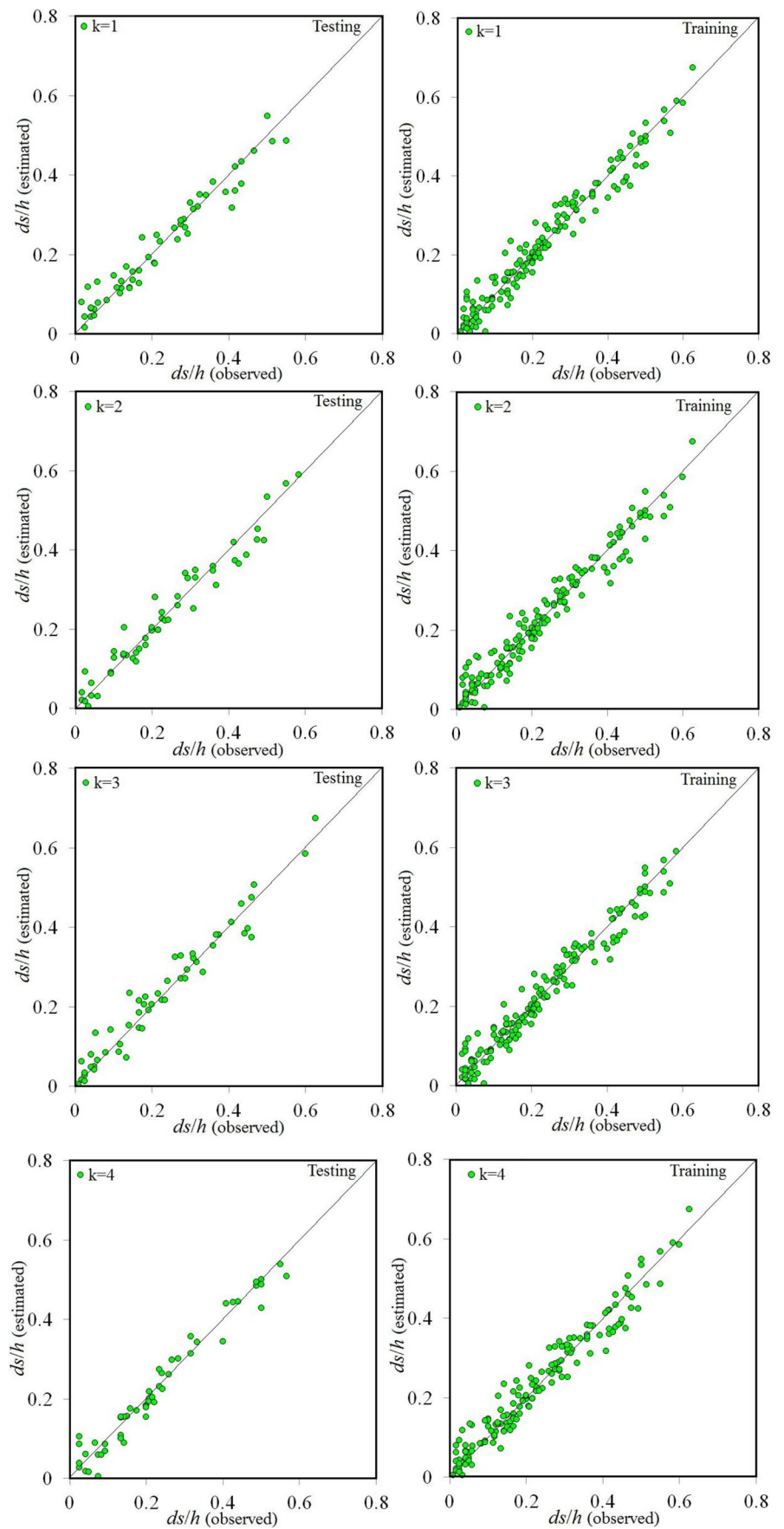
### Uncertainty analysis

The uncertainty analysis of ORELM models is performed in this section to evaluate the projected error by numerical models and to assess their performance. In general, the numerical model's predicted error is equal to the numerical model's simulated values ( $P_i$ ) minus the observational values. ( $O_i$ ) ( $e_i = P_i - O_i$ ). Also, the average of the predicted error is calculated as  $\bar{e} = \sum_{i=1}^n e_i$ . In addition, the standard deviation of the predicted error values is  $S_e = \sqrt{\sum_{i=1}^n (e_i - \bar{e})^2 / n - 1}$ . It should be noted that the negative and positive values of  $\bar{e}$  indicate that the numerical model has an underestimated and overestimated performance, respectively. Also, using parameters of  $\bar{e}$  and  $S_e$ , a confidence band is plotted around the predicted error values by Wilson score's method without continuity correction, then, using  $\pm 1.64S_e$  approximately

**Fig. 7** Schematic of  $k$ -fold cross-validation method for  $k=4$



**Fig. 8** Scatter plot for  $k=4$  in the  $k$ -fold cross-validation method



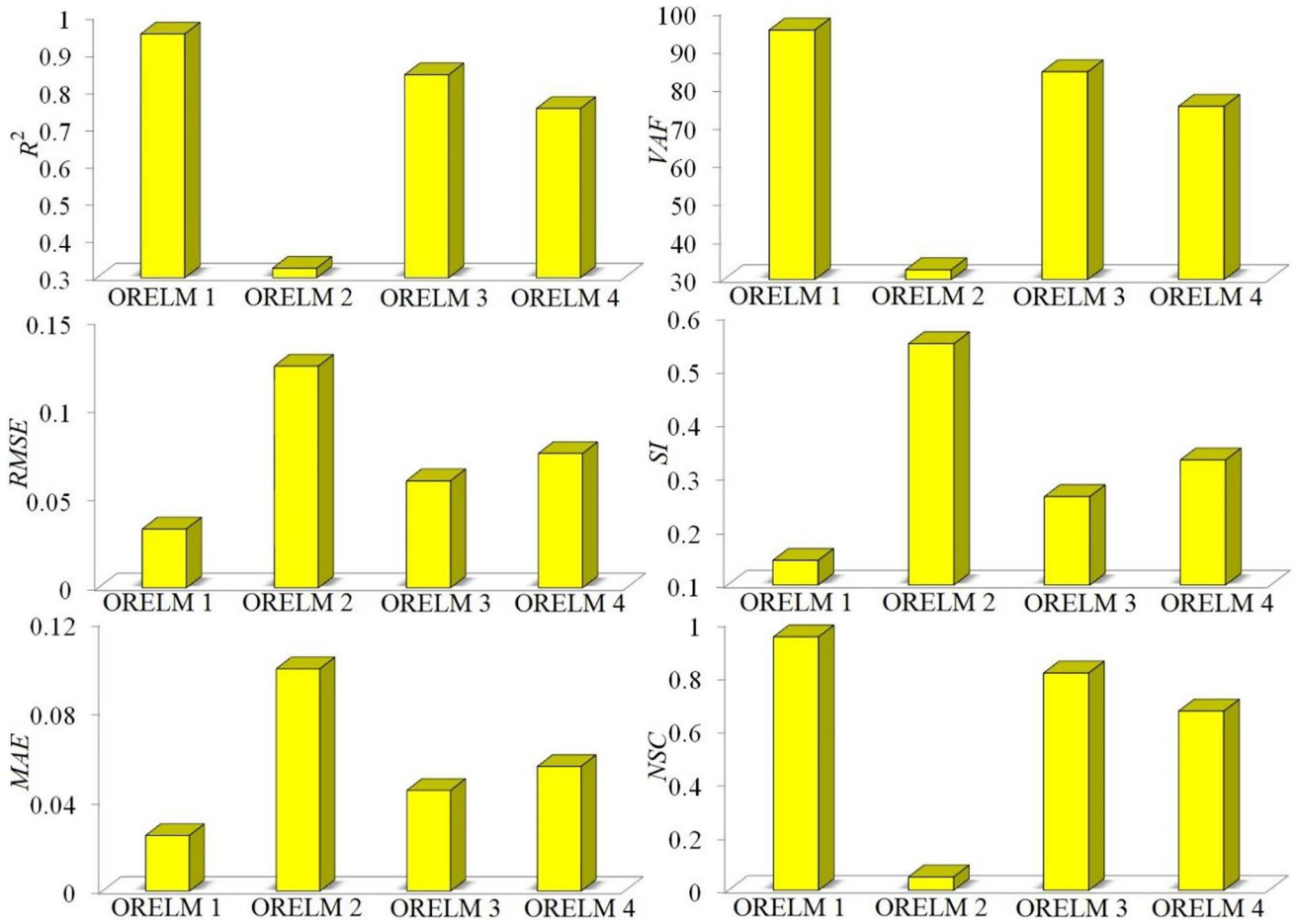


Fig. 9 Results of statistical indices for different ORELM models

95% band, which shown with 95% PEI. Table 3 shows the parameters for the improved model’s uncertainty analysis. The WUB represents the breadth of the uncertainty band in this table. The ORELM1, ORELM2, and ORELM4 models have underestimated performance, while the ORELM3 model has overestimated performance, according to the results of the uncertainty analysis. In addition, the 95% PEI value used by the ORELM1 model to estimate scour depth is between  $-0.005$  and  $0.004$ . In the meantime, the ORELM2 uncertainty band is around  $-0.017$  wide. Furthermore, the value of  $Se$  for the ORELM3 and ORELM4 models is predicted to be  $0.06$  and  $0.076$ , respectively.

As a result of the modeling results analysis, the ORELM1 model is chosen as the superior model for estimating scour depth in the region of the twin and three piers. A relationship is constructed for this model as follows:

$$\frac{d_s}{h} = \left| \left[ \frac{1}{(1 + \exp(\ln W \times \ln V + BHN))} \right]^T \times OutW \right|. \quad (28)$$

The input weights matrix is  $\ln W$ , the input variables matrix is  $\ln V$ , the bias-layer neuron matrix is  $BHN$ , and the output weights matrix is  $OutW$ . Furthermore, the best values for these matrices are listed below:

$$\ln V = \begin{bmatrix} D/h \\ d/h \\ Fr \end{bmatrix} \quad BHN = \begin{bmatrix} 0.047 \\ -0.028 \\ 0.223 \\ -0.720 \\ 0.234 \\ 0.655 \\ -0.116 \\ -0.178 \\ -0.068 \\ -0.879 \\ -0.873 \\ -0.066 \\ 0.602 \\ 0.101 \\ -0.833 \\ 0.857 \\ -0.657 \end{bmatrix} \quad \ln W = \begin{bmatrix} -0.774 & -0.789 & 0.918 \\ 0.386 & -0.807 & -0.297 \\ 0.983 & 0.573 & -0.657 \\ 0.065 & -0.876 & -0.551 \\ -0.640 & 0.665 & 0.757 \\ -0.480 & -0.246 & 0.455 \\ -0.407 & -0.354 & -0.048 \\ -0.370 & 0.876 & -0.495 \\ -0.141 & 0.335 & 0.335 \\ -0.844 & -0.999 & 0.214 \\ 0.277 & 0.513 & 0.463 \\ 0.630 & -0.818 & 0.931 \\ -0.361 & -0.040 & 0.699 \\ 0.368 & 0.777 & 0.807 \\ 0.478 & 0.939 & 0.848 \\ -0.249 & 0.595 & -0.209 \\ -0.401 & -0.155 & 0.746 \end{bmatrix} \quad OutW = \begin{bmatrix} 73.924 \\ 214.041 \\ 84.575 \\ -219.899 \\ 105.166 \\ -52.979 \\ 180.606 \\ 35.214 \\ -48.781 \\ -71.814 \\ 107.885 \\ -75.918 \\ 81.121 \\ -194.716 \\ 92.059 \\ -216.919 \\ -57.742 \end{bmatrix} \quad (29)$$

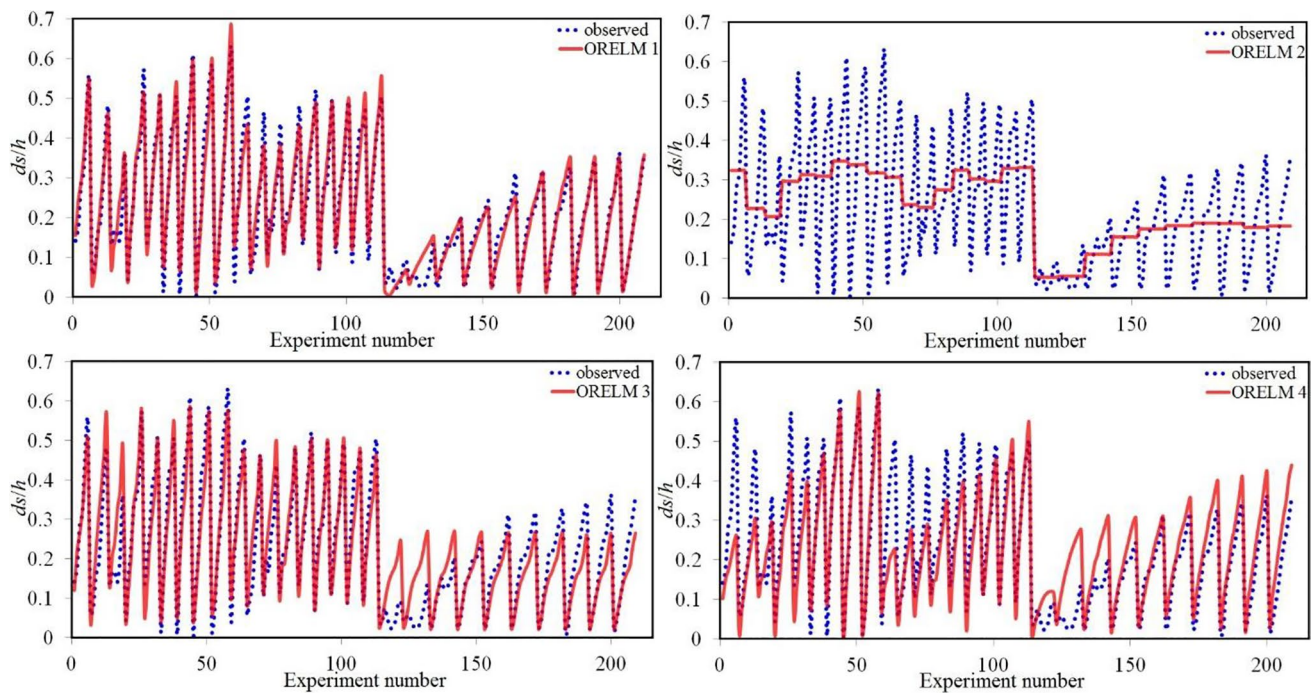


Fig. 10 Comparison of observed and simulated scour depths by different ORELM models

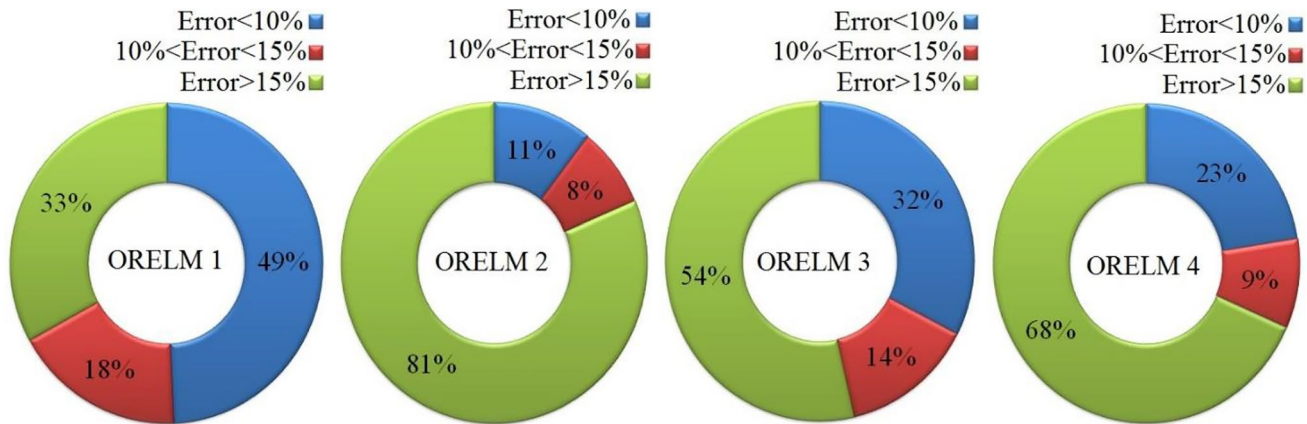


Fig. 11 Error distribution for different ORELM models

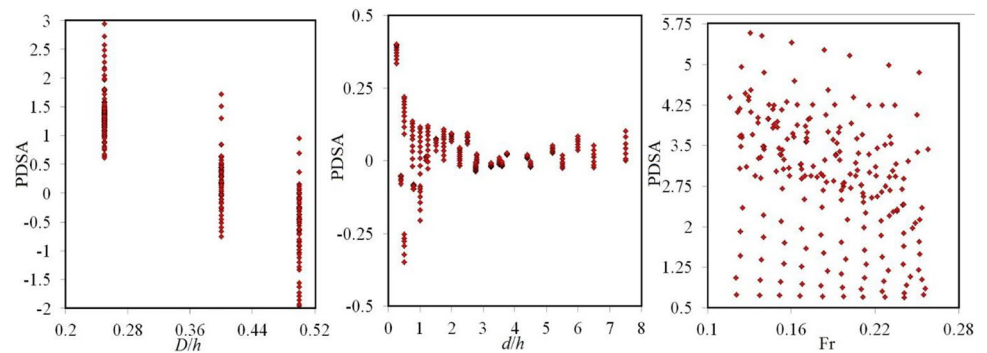
**Partial derivative sensitivity analysis (PDSA)**

The partial derivative sensitivity analysis (PDSA) is applied to the superior model (ORELM1) in this section, and the input parameters are evaluated. In general, one of the most essential methods for determining the pattern of fluctuation of input parameters is partial derivative sensitivity analysis (PDSA) (Azimi et al., 2017). Furthermore, a positive partial derivative sensitivity analysis indicates

**Table 3** Uncertainty analysis parameters for different ORELM models

Model	Number of samples	$\bar{e}$	$S_e$	WUB	95% PEI
ORELM 1	209	-0.008	0.033	-0.005	-0.005 to 0.004
ORELM 2	209	-1.423E-09	0.125	-0.017	-0.017 to 0.017
ORELM 3	209	1.0126E-06	0.060	-0.008	-0.008 to 0.008
ORELM 4	209	-3.424E-05	0.076	-0.01	-0.010 to 0.010

**Fig. 12** The results of PDSA for the ORELM superior model



that the objective function (scour) is increasing; on the other hand, a negative value indicates that the output value is decreasing. The ratio of the objective function is used to derive the relative derivative of each input parameter in this study. In other words, for each input variable, the relative derivative  $f(x)$  is determined (Fig. 12). The value of PDSA, for example, diminishes as  $D/h$  increases. For  $d/h$  greater than 4, however, the scour depth increases, and the  $d/h$  (as the input parameter) increases. Furthermore, with increasing  $Fr$ , the PDSA pattern displays a declining trend.

## Conclusion

The scour depth around twin and three piers were simulated using a new outlier robust extreme learning machine (ORELM) in this work.  $k$ -fold cross-validation for  $k=4$  was performed to validate the simulation findings. The ideal number of hidden layer neurons and activation function was chosen at first. In other words, the sigmoid function and several ideal neurons of 17 were introduced as optimal activation. Following that, four ORELM models were created utilizing the input parameters. Analyzing the modeling results revealed the superior model and the most effective input parameters. The superior model simulated the scouring values with acceptable accuracy. The optimal values for all input parameters were estimated using this model, and the most effective input parameters were  $Fr$  and  $D/h$ . For ORELM1 (superior model), the RMSE, MAE, and VAF values were calculated to be 0.033, 0.025, and 95.249, respectively. Furthermore, the error distribution revealed that approximately 18% of the ORELM model's outputs had an error of between 10 and 15%. In addition, an uncertainty analysis was done on all ORELM models, and the ORELM1 model underperformed. It should be mentioned that for the ORELM1 model, a simple equation was presented for engineers

to employ in their practical work. Finally, a PDSA was used to solve this problem.

**Acknowledgements** The author would like to thank Shahid Chamran University of Ahvaz for their support.

**Author contribution** Writing original draft: MRGN; methodology: AF; analysis: AP; writing review and editing: SDL.

**Data availability** Not applicable.

**Code availability** Not applicable.

## Declarations

**Ethics approval** Not applicable.

**Consent to participate** Not applicable.

**Consent for publication** Not applicable.

**Conflict of interest** The authors declare no competing interests.

## References

- Amini A, Melville BW, Ali TM, Ghazali AH (2012) Clear-water local scour around pile groups in shallow-water flow. *J Hydraul Eng* 138(2):177–185. [https://doi.org/10.1061/\(asce\)hy.1943-7900.0000488](https://doi.org/10.1061/(asce)hy.1943-7900.0000488)
- AminiBaghbadorani D, Ataie-Ashtiani B, Beheshti A, Hadjzaman M, Jamali M (2018) Prediction of current-induced local scour around complex piers: review, revisit, and integration. *Coast Eng* 133(December 2017):43–58. <https://doi.org/10.1016/j.coastaleng.2017.12.006>
- AminiBaghbadorani D, Beheshti AA, Ataie-Ashtiani B (2017) Scour hole depth prediction around pile groups: review, comparison of existing methods, and proposition of a new approach. *Nat Hazards* 88(2):977–1001. <https://doi.org/10.1007/s11069-017-2900-9>
- Ataie-Ashtiani B, Aslani-Kordkandi A (2012) Flow field around side-by-side piers with and without a scour hole. *Eur J Mech B Fluids* 36:152–166. <https://doi.org/10.1016/j.euromechflu.2012.03.007>
- Ataie-Ashtiani B, Baratian-Ghorghi Z, Beheshti AA (2010) Experimental investigation of clear-water local scour of compound piers. *J Hydraul Eng* 136(6):343–351. [https://doi.org/10.1061/\(ASCE\)0733-9429\(2010\)136:6\(343\)](https://doi.org/10.1061/(ASCE)0733-9429(2010)136:6(343))

- Azimi H, Bonakdari H, Ebtehaj I, Ashraf Talesh SH, Michelson DG, Jamali A (2017) Evolutionary Pareto optimization of an ANFIS network for modeling scour at pile groups in clear water condition. *Fuzzy Sets Syst* 319:50–69. <https://doi.org/10.1016/j.fss.2016.10.010>
- Bazrafshan O, Ehteram M, Dashti Latif S, Feng Huang Y, YennTeo F, Najah Ahmed A, El-Shafie A (2022) Predicting crop yields using a new robust Bayesian averaging model based on multiple hybrid ANFIS and MLP models: predicting crop yields using a new robust Bayesian averaging model. *Ain Shams Eng J* 13(5):101724. <https://doi.org/10.1016/j.asej.2022.101724>
- Bozkus Z, Özalp MC, Dinçer AE (2018) Effect of pier inclination angle on local scour depth around bridge pier groups. *Arab J Sci Eng* 43(10):5413–5421. <https://doi.org/10.1007/s13369-018-3141-2>
- Coleman SE (2005) Clearwater local scour at complex piers. *J Hydraul Eng* 131(4):330–334. [https://doi.org/10.1061/\(asce\)0733-9429\(2005\)131:4\(330\)](https://doi.org/10.1061/(asce)0733-9429(2005)131:4(330))
- Das S, Das R, Mazumdar A (2016) Comparison of local scour characteristics around two eccentric piers of different shapes. *Arab J Sci Eng* 41(4):1199–1213. <https://doi.org/10.1007/s13369-015-1817-4>
- Ebtehaj I, Bonakdari H, Moradi F, Gharabaghi B, Khozani ZS (2018) An integrated framework of Extreme Learning Machines for predicting scour at pile groups in clear water condition. *Coast Eng* 135(June 2017):1–15. <https://doi.org/10.1016/j.coastaleng.2017.12.012>
- Ebtehaj I, Bonakdari H, Shamshirband S (2016) Extreme learning machine assessment for estimating sediment transport in open channels. *Eng Comput* 32(4):691–704. <https://doi.org/10.1007/s00366-016-0446-1>
- Ehteram M, Ahmed AN, Latif SD, Huang YF, Alizamir M, Kisi O et al (2020) Design of a hybrid ANN multi-objective whale algorithm for suspended sediment load prediction. *Environ Sci Pollut Res*. <https://doi.org/10.1007/s11356-020-10421-y>
- Etemad-Shahidi A, Bonakdar L, Jeng DS (2015) Estimation of scour depth around circular piers: applications of model tree. *J Hydroinf* 17(2):226–238. <https://doi.org/10.2166/hydro.2014.151>
- Harasti A, Gilja G, Potočki K, Lacko M (2021) Scour at bridge piers protected by the riprap sloping structure: A review. *Water (Switzerland)*, 13(24). <https://doi.org/10.3390/w13243606>
- Horata P, Chiewchanwattana S, Sunat K (2013) Robust extreme learning machine. *Neurocomputing* 102:31–44. <https://doi.org/10.1016/j.neucom.2011.12.045>
- Huang GB, Zhu QY, Siew CK (2004) Extreme learning machine: a new learning scheme of feedforward neural networks. *IEEE Int Conf Neural Netw Conf Proc* 2:985–990. <https://doi.org/10.1109/IJCNN.2004.1380068>
- Latif SD (2021a) Concrete compressive strength prediction modeling utilizing deep learning long short-term memory algorithm for a sustainable environment. *Environ Sci Pollut Res*. <https://doi.org/10.1007/s11356-021-12877-y>
- Latif SD (2021b) Developing a boosted decision tree regression prediction model as a sustainable tool for compressive strength of environmentally friendly concrete. *Environ Sci Pollut Res*. <https://doi.org/10.1007/s11356-021-15662-z>
- Latif SD, Ahmed AN (2021) Application of deep learning method for daily streamflow time-series prediction : a case study of the Kowmung River at Cedar Ford, Australia. *Int J Sustain Dev Plan* 16(3):497–501. <https://doi.org/10.18280/ijstdp.160310>
- Latif SD, Ahmed AN, Sathiamurthy E, Huang YF, El-Shafie A (2021a) Evaluation of deep learning algorithm for inflow forecasting: a case study of Durian Tunggal Reservoir, Peninsular Malaysia. *Nat Hazards*, (0123456789). <https://doi.org/10.1007/s11069-021-04839-x>
- Latif SD, Azmi MSBN, Ahmed AN, Fai CM, El-Shafie A (2020) Application of artificial neural network for forecasting nitrate concentration as a water quality parameter: a case study of Feitsui Reservoir, Taiwan. *Int J Des Nat Ecodynamics*. <https://doi.org/10.18280/ijdne.150505>
- Latif SD, Birima AH, Najah A, Mohammed D, Al-ansari N, Ming C, El-shafie A (2021b) Development of prediction model for phosphate in reservoir water system based machine learning algorithms. *Ain Shams Eng J*. <https://doi.org/10.1016/j.asej.2021.06.009>
- Liang F, Wang C, Huang M, Wang Y (2017) Experimental observations and evaluations of formulae for local scour at pile groups in steady currents. *Mar Georesour Geotechnol* 35(2):245–255. <https://doi.org/10.1080/1064119X.2016.1147510>
- Liang NY, Huang GB, Saratchandran P, Sundararajan N (2006) A fast and accurate online sequential learning algorithm for feedforward networks. *IEEE Trans Neural Networks* 17(6):1411–1423. <https://doi.org/10.1109/TNN.2006.880583>
- Link O, Mignot E, Roux S, Camenen B, Escauriaza C, Chauchat J, et al (2019) Scour at bridge foundations in supercritical flows: an analysis of knowledge gaps. *Water (Switzerland)*, 11(8). <https://doi.org/10.3390/w11081656>
- Melville B, Coleman S, Priestley S (2007) Local scour at complex piers. Examining the Confluence of Environmental and Water Concerns—Proceedings of the World Environmental and Water Resources Congress 2006, (Figure 1). [https://doi.org/10.1061/40856\(200\)176](https://doi.org/10.1061/40856(200)176)
- Moreno M, Maia R, Couto L (2016) Effects of relative column width and pile-cap elevation on local scour depth around complex piers. *J Hydraul Eng* 142(2):04015051. [https://doi.org/10.1061/\(asce\)hy.1943-7900.0001080](https://doi.org/10.1061/(asce)hy.1943-7900.0001080)
- Muzzammil M, Alama J, Danish M (2015) Scour prediction at bridge piers in cohesive bed using gene expression programming. *Aquatic Procedia*, 4(Icwrcoe), 789–796. <https://doi.org/10.1016/j.aqpro.2015.02.098>
- Najah A, Teo FY, Chow MF, Huang YF, Latif SD, Abdullah S et al (2021) Surface water quality status and prediction during movement control operation order under COVID-19 pandemic: case studies in Malaysia. *Int J Environ Sci Technol*. <https://doi.org/10.1007/s13762-021-03139-y>
- Parsaie A, Haghiabi AH, Latif SD (2021) Predictive modelling of piezometric head and seepage discharge in earth dam using soft computational models. *Environ Sci Pollut Res*. <https://doi.org/10.1007/s11356-021-15029-4>
- Parsaie A, Haghiabi AH (2017) Mathematical expression of discharge capacity of compound open channels using MARS technique. *J Earth Syst Sci* 126(2):20. <https://doi.org/10.1007/s12040-017-0807-1>
- Wang H, Tang H, Liu Q, Wang Y (2016a) Local scouring around twin bridge piers in open-channel flows. *J Hydraul Eng* 142(9):06016008. [https://doi.org/10.1061/\(asce\)hy.1943-7900.0001154](https://doi.org/10.1061/(asce)hy.1943-7900.0001154)
- Wang H, Tang HW, Xiao JF, Wang Y, Jiang S (2016b) Clear-water local scouring around three piers in a tandem arrangement. *SCI-ENCE CHINA Technol Sci* 59(6):888–896. <https://doi.org/10.1007/s11431-015-5905-1>
- Zhang K, Luo M (2015) Outlier-robust extreme learning machine for regression problems. *Neurocomputing* 151(P3):1519–1527. <https://doi.org/10.1016/j.neucom.2014.09.022>

**Publisher's note** Springer Nature remains neutral with regard to jurisdictional claims in published maps and institutional affiliations.